Microchimica Acta (2022) 189:464
https://doi.org/10.1007/s00604-022-05551-8

ORIGINAL PAPER

Preparation of complex biological sample-compatible "turn-on"-type ratiometric fluorescent molecularly imprinted polymer microspheres via one-pot surface-initiated ATRP

Qun Li[1] · Wanlan Zhang[1] · Xinru Liu[1] · Huiqi Zhang[1]

Received: 5 August 2022 / Accepted: 25 October 2022 / Published online: 23 November 2022

Abstract

The efficient preparation of ratiometric fluorescent molecularly imprinted polymer (MIP) microspheres that can directly and selectively optosense a herbicide (i.e., 2,4-dichlorophenoxyacetic acid, 2,4-D) in undiluted pure milk is described. The dual fluorescent MIP microparticles were readily obtained through grafting a green 4-nitrobenzo[c][1,2,5]oxadiazole (NBD)-labeled 2,4-D-MIP layer with hydrophilic polymer brushes onto the preformed uniform "living" red CdTe quantum dot (QD)-labeled SiO_2 microspheres via one-pot surface-initiated atom transfer radical polymerization (SI-ATRP) in the presence of a polyethylene glycol macro-ATRP initiator. They proved to be highly promising "turn-on"-type fluorescent chemosensors with red CdTe QD (the maximum emission wavelength $\lambda_{e,max}$ around 710 nm) and green NBD ($\lambda_{e,max}$ around 515 nm) as the reference fluorophore and "turn-on"-type responsive fluorophore, respectively. The sensors showed excellent photostability and reusability, high 2,4-D selectivity and sensitivity (the limit of detection = 0.12 μM), and direct visual detection ability (a fluorescent color change occurs from red to blue-green with the concentration of 2,4-D increasing from 0 to 100 μM) in pure bovine milk. The sensors were used for 2,4-D detection with high recoveries (96.0–104.0%) and accuracy (RSD ≤ 4.0%) in pure goat milk at three spiking levels of both 2,4-D and its mixtures with several analogues. This new strategy lays the foundation for efficiently developing diverse complex biological sample-compatible ratiometric fluorescent MIPs highly useful for real-world bioanalyses and diagnostics.

Keywords Molecularly imprinted polymers · Complex biological samples · Fluorescence "turn-on" · Optosensors · One-pot surface-initiated ATRP

Introduction

Molecularly imprinted polymers (MIPs) are biomimetic receptors with tailor-made target analyte binding sites [1–6]. Their highly stable, easily preparable, and cheap attributes make them promising synthetic substitutes for biological receptors in many applications. Fluorescent MIP-based chemosensors with the combined advantages of MIPs and fluorescent analyses [7] have attracted tremendous interest owing to their great potential in the bioanalytical and biomedical fields [8–13]. Among them, the ratiometric fluorescent MIP sensors (typically with dual fluorescence) have received particular attention because of their excellent self-referencing capability (thus eliminating external interferences) and direct visual detection ability [12]. Despite some progress made in the development of ratiometric fluorescent MIPs capable of optosensing small organic analytes in simple aqueous samples (e.g., tap water [14, 15], lake/river water [14, 15], or seawater [16]), they normally failed to work in real undiluted complex biological samples. This drawback greatly limits their real-world bioanalytical and biomedical applications. Note that although some ratiometric fluorescent MIPs were reported to be able to optosense small organic analytes in complex biological samples [17–20], certain sample pretreatment procedures (e.g., removing proteins from biological samples [17, 18] or high dilution [19, 20]) were always required prior to the optosensing, which are either time-consuming or make the

✉ Huiqi Zhang
zhanghuiqi@nankai.edu.cn

[1] State Key Laboratory of Medicinal Chemical Biology, Key Laboratory of Functional Polymer Materials (Ministry of Education), Collaborative Innovation Center of Chemical Science and Engineering (Tianjin), College of Chemistry, Nankai University, Tianjin 300071, China

optosensing of biological samples with low analyte concentrations more difficult or even impossible (because high dilution largely decreases analyte concentrations).

Recently, our group has developed some ratiometric fluorescent MIPs that can directly and selectively optosense small organic analytes in real undiluted complex biological samples through their controlled surface-grafting of hydrophilic polymer brushes (leading to their largely reduced nonspecific bindings and enhanced antifouling ability in complex biological samples) [21, 22]. For instance, we prepared ratiometric fluorescent MIP microspheres for directly and selectively optosensing a widely used herbicide (i.e., 2,4-dichlorophenoxyacetic acid, 2,4-D) in the undiluted pure milks via RAFT coupling chemistry (2,4-D detection is highly important because it can disrupt endocrine activities and has been frequently found in the environmental water and "weed and feed" products) [21]. Their synthesis involved first the successive grafting of a red CdTe quantum dot (QD)-labeled polymer layer and a green 4-nitrobenzo[c][1,2,5]oxadiazole (NBD)-labeled 2,4-D-MIP layer onto the preformed "living" polymer particles with surface-bound dithioester groups (prepared by using RAFT precipitation polymerization [23]) via two-step surface-initiated RAFT polymerization (with CdTe QD as the reference fluorophore and NBD as the "turn-on"-type responsive fluorophore) and the subsequent grafting of hydrophilic poly(*N*-isopropylacrylamide) brushes via an efficient coupling reaction [24]. They showed dramatic "turn-on"-type ratiometric fluorescence and color changes upon exposing to 2,4-D and high 2,4-D optosensing selectivity and sensitivity in the undiluted pure milks. In another work, we also developed complex biological sample-compatible "turn-on"-type ratiometric fluorescent 2,4-D-MIP microspheres with high 2,4-D selectivity and sensitivity in the undiluted pure milks [22]. They were prepared through successively grafting a green NBD-labeled 2,4-D-MIP layer and hydrophilic poly(glyceryl monomethacrylate) (PGMMA) brushes onto the preformed "living" red CdTe QD-labeled silica particles with surface-bound alkyl bromide groups (i.e., ATRP-initiating groups) (by using the one-pot sol–gel reaction) via two-step surface-initiated atom transfer radical polymerization (ATRP) (SI-ATRP). The obvious optosensing advantage of these ratiometric fluorescent MIPs (i.e., not requiring any complex biological sample pretreatment), together with their much reduced false-positive responses and higher sensitivity owing to their "turn-on"-type fluorescent attribute [25], makes them highly promising optosensors for directly and selectively detecting the herbicide in the undiluted pure milks. Nevertheless, their multi-step syntheses largely limit their large-scale productions. Particularly, although SI-ATRP has proven highly versatile for grafting various MIP layers and hydrophilic polymer brushes onto "living" particles [26], the Cu(II) species existing in SI-ATRP systems [including those generated by the "persistent radical effect" (i.e., Cu(II) and free radical are simultaneously produced by reacting alkyl halide and Cu(I) in the beginning of ATRP) [27] and those added into the ATRP system for better controlling the grafting of hydrophilic polymer brushes [28]] showed large quenching effect on the fluorescence of CdTe QD-labeled silica particles. The use of two-step SI-ATRP required rather complicated reaction condition optimization to obtain ratiometric fluorescent MIPs with proper dual fluorescence intensities (i.e., reducing the Cu(I) amount for SI-ATRPs as well as keeping the template embedded inside the MIP particles and not adding Cu(II) during grafting PGMMA brushes) [22]. Therefore, the development of a versatile new strategy for efficiently obtaining "turn-on"-type ratiometric fluorescent MIPs fully compatible with complex biological samples is highly desirable.

In this manuscript, an efficient one-pot SI-ATRP strategy is described for preparing "turn-on"-type ratiometric fluorescent MIP microspheres capable of directly and selectively optosensing 2,4-D in the undiluted pure milks (Fig. 1). It involves the controlled grafting of a green NBD-labeled 2,4-D-MIP layer with hydrophilic polymer brushes onto the preformed uniform "living" red CdTe QD-labeled silica microparticles with surface-bound alkyl bromide groups (prepared by using one-pot sol–gel reaction) via one-pot SI-ATRP in the presence of a polyethylene glycol (PEG) macro-ATRP initiator [PEG-Br (Fig. 1(d))]. The morphologies, particle sizes and size distributions, chemical structures, surface hydrophilicity, and equilibrium/competitive-binding properties of the resulting dual fluorescent 2,4-D-MIP particles were characterized in detail. In addition, their direct and highly selective optosensing and accurate quantification of 2,4-D in the undiluted pure milks were also demonstrated. This new strategy opens the door for efficiently developing various complex biological sample-compatible ratiometric fluorescent MIPs highly useful in practical bioanalyses and diagnostics.

Experimental section

Chemicals and materials

The chemicals and materials utilized in this work are described in the Supporting Information.

Preparation of the grafted dual fluorescent 2,4-D-imprinted polymer (2,4-D-MIP)/non-imprinted polymer [or control polymer (2,4-D-CP)] particles (i.e., rQD-SiO_2@NBD-MIP@PEG and rQD-SiO_2@NBD-CP@PEG, entries 4 and 5 in Table 1).

The grafted dual fluorescent 2,4-D-MIP particles (i.e., dual fluorescent 2,4-D-MIP particles with surface-grafted PEG brushes) were prepared via one-pot SI-ATRP in the

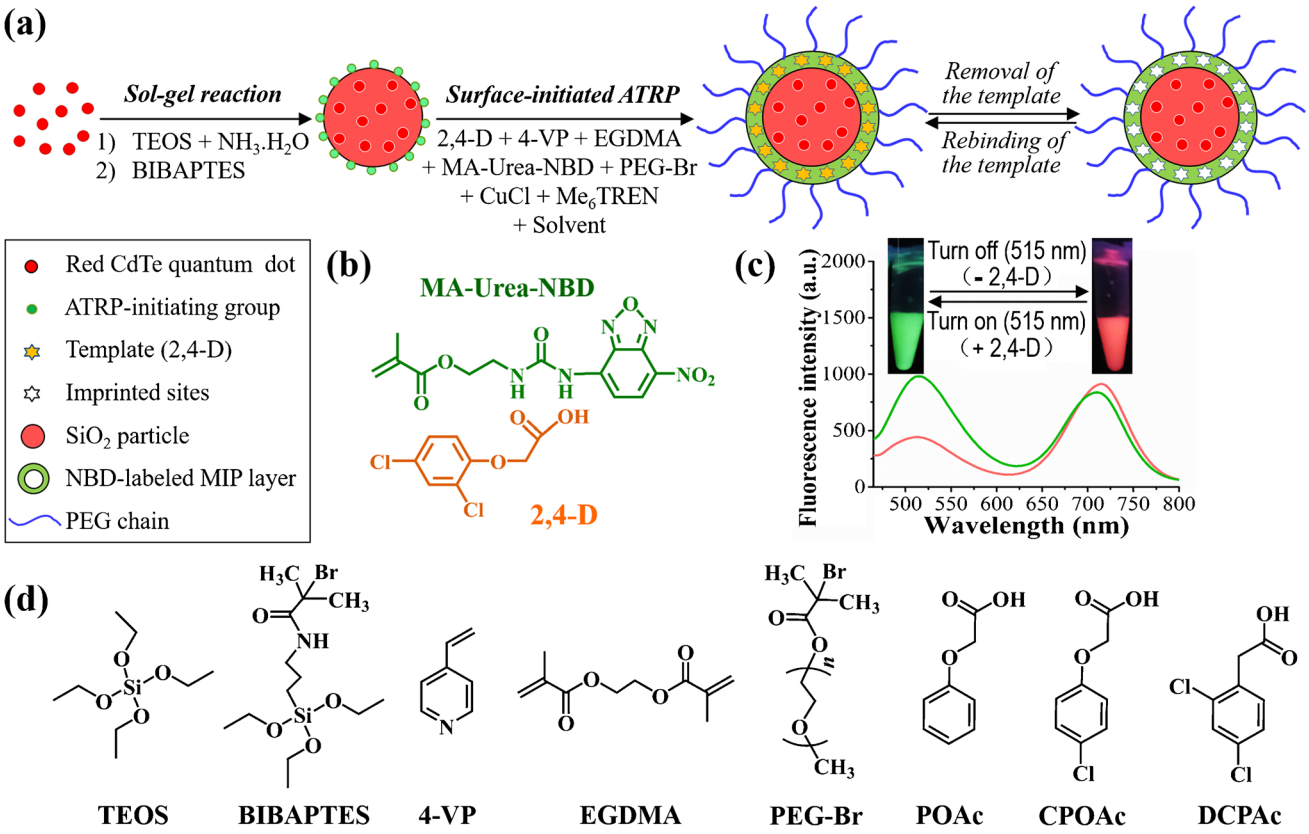

Fig. 1 (**a**) Schematic illustration for preparing "turn-on"-type ratiometric fluorescent MIP microparticles with PEG brushes via one-pot SI-ATRP. (**b**) The non-covalent complex formed between MA-Urea-NBD and 2,4-D through hydrogen-bonding interaction. (**c**) Fluorescent spectra and fluorescence colors (under 365 nm UV light irradiation) of the ratiometric fluorescent 2,4-D-MIP with PEG brushes (red) and its mixture with 2,4-D (green) in the undiluted pure bovine milk. (**d**) Chemical structures of some reagents utilized in this work

Table 1 Synthetic and characterization data of the "living" red CdTe QD-labeled silica particles and both the grafted and ungrafted dual fluorescent 2,4-D-MIP/CP particles

Entry	Sample	ΔW (%) [a]	$D_{n,AFM}$ (nm) [b]	U [b]	$D_{n,DLS}$ (nm) [c]	PDI [c]	Contact angle (°) [d]
1	rQD-SiO_2-Br	-	651	1.010	694	0.155	59.1 ± 2.3
2	rQD-SiO_2@NBD-MIP	11.3	673	1.012	719	0.131	124.4 ± 2.8
3	rQD-SiO_2@NBD-CP	12.1	676	1.007	717	0.156	123.0 ± 3.2
4	rQD-SiO_2@NBD-MIP@PEG	21.4	692	1.005	753	0.137	60.2 ± 1.5
5	rQD-SiO_2@NBD-CP@PEG	20.7	694	1.011	752	0.107	58.1 ± 1.6

[a]Enhanced weight percentage of MIP/CP particles (obtained via surface modification) compared with the starting rQD-SiO_2-Br particles; [b]$D_{n,AFM}$ and U refer to the number-average diameter and size distribution index of the particles determined by AFM, respectively; [c]$D_{n,DLS}$ and PDI denote the number-average hydrodynamic diameter and particle dispersion index of the particles determined by DLS, respectively; [d]the static water contact angles of the sample films

presence of PEG-Br with the "living" red CdTe QD-labeled silica particles (i.e., rQD-SiO_2-Br, entry 1 in Table 1) (see their preparation in the Supporting Information) as the immobilized ATRP initiator as follows: to a one-neck round-bottom flask (100 mL) with a magnetic stir bar inside were added 4-vinylpyridine (4-VP) (0.71 mmol), 2,4-D (0.35 mmol), 2-(3-(4-nitrobenzo[c][1,2,5]oxadiazo-7-yl)ureido)ethyl methacrylate (MA-Urea-NBD) (0.023 mmol), and dried acetonitrile (72 mL) successively. The above solution was first stirred in an ice-water bath for 2 h and then put into a refrigerator (4 °C) overnight to allow the self-assembly of the functional monomers and template. Afterwards, the reaction flask containing the above reaction mixture was put into an ice-water bath, and ethylene glycol dimethacrylate (EGDMA) (2.11 mmol) and tris(2-(dimethylamino)ethyl) amine (Me_6TREN) (0.127 mmol) were added successively.

After the above reaction mixture was bubbled with argon for 15 min in an ice-water bath, CuCl (0.017 mmol) was added. After another 15 min of argon bubbling through the reaction mixture, the "living" rQD-SiO_2-Br particles (70 mg) and PEG-Br (58.3 mg) was added into the reaction system. The above mixture was further bubbled with argon for 5 min, sealed, and magnetically stirred (300 rpm) at 60 °C for 28 h. The product was centrifuged, washed with methanol 7 times at 40 °C, and then dried at 40 °C under vacuum to a constant weight, resulting in the grafted dual fluorescent 2,4-D-MIP particles with a weight increase of 21.4% in comparison with the starting "living" rQD-SiO_2-Br particles (entry 4, Table 1).

The grafted dual fluorescent 2,4-D-CP particles were also prepared and purified under the identical conditions except for omitting 2,4-D. They showed a weight increase of 20.7% compared with the starting "living" rQD-SiO_2-Br particles (entry 5, Table 1).

Preparation of the ungrafted dual fluorescent 2,4-D-MIP/CP particles (i.e., rQD-SiO_2@NBD-MIP and rQD-SiO_2@NBD-CP, entries 2 and 3 in Table 1)

The ungrafted dual fluorescent 2,4-D-MIP and 2,4-D-CP particles (i.e., dual fluorescent 2,4-D-MIP and 2,4-D-CP particles without PEG brushes) were prepared similarly as for the grafted dual fluorescent 2,4-D-MIP and 2,4-D-CP particles except for omitting PEG-Br during the SI-ATRP processes. They showed a weight increase of 11.3% and 12.1% compared with the starting "living" rQD-SiO_2-Br particles, respectively (entries 2 and 3 in Table 1).

Characterization

The samples were characterized with ^{1}H NMR spectrometer, FT-IR spectrometer, atomic force microscope (AFM), and dynamic light scattering (DLS). The details of the instruments and characterization are included in the Supporting Information.

The detailed information for studying the static water contact angles of the films prepared with the obtained particles and the equilibrium/competitive binding properties of the ungrafted and grafted dual fluorescent 2,4-D-MIPs/2,4-D-CPs is presented in the Supporting Information.

An F-4600 spectrofluorometer (Hitachi, Japan) was used to investigate the optosensing behaviors of the ratiometric fluorescent 2,4-D-MIP/CP particles by recording the fluorescence emission spectra of their solutions or their mixed solutions with analyte(s) (the excitation wavelength was 420 nm, the voltage was 600 V, and the slit width of both the excitation and emission was 10 nm; the fluorescence intensities of NBD fluorophores around 515 nm and those of CdTe QDs around 710 nm were selected for the optosensing analyses).

The detailed information for studying the photostability/reusability and the binding kinetics of the grafted dual fluorescent 2,4-D-MIP/CP as well as the optosensing of 2,4-D with the grafted dual fluorescent 2,4-D-MIP/CP in the undiluted pure milk(s) is also presented in the Supporting Information.

Results and discussion

Synthesis and characterization of hydrophilic "turn-on"-type ratiometric fluorescent 2,4-D-MIP/CP particles (briefly the grafted dual fluorescent 2,4-D-MIP/CP)

To demonstrate the proof-of-principle of our one-pot SI-ATRP new strategy for developing "turn-on"-type ratiometric fluorescent MIPs fully compatible with real undiluted complex biological samples, we chose the herbicide 2,4-D as the target small organic analyte, red CdTe QD as the reference fluorophore (owing to its inertness toward 2,4-D), and green NBD as the responsive fluorophore (due to its fluorescence "light up" effect toward 2,4-D) (Fig. 1) [21, 22]. The dual fluorescent 2,4-D-MIP particles with PEG brushes [briefly the grafted (dual fluorescent) 2,4-D-MIP] (i.e., rQD-SiO_2@NBD-MIP@PEG, entry 4 in Table 1) were readily obtained through the controlled surface-grafting of a green NBD-labeled fluorescent 2,4-D-MIP layer with PEG brushes onto the preformed "living" red CdTe QD-labeled silica microspheres (i.e., rQD-SiO_2-Br particles, entry 1 in Table 1) (see their synthesis in the Supporting Information [26]) via one-pot SI-ATRP. 2,4-D, 4-VP, MA-Urea-NBD, EGDMA, and PEG-Br (Figs. 1(b,d) and S1) were utilized as the template, functional monomer, fluorescent comonomer, cross-linker, and hydrophilic macro-ATRP initiator, respectively, according to our previous reports [21, 22]. Both the pyridine unit of 4-VP and the ureido unit of MA-Urea-NBD can form hydrogen-bonding interactions with the carboxylic group of 2,4-D, thus leading to imprinted binding sites with pyridine and/or ureido unit(s) inside the MIP layer that can selectively interact with 2,4-D. The grafted dual fluorescent control polymer particles (i.e., rQD-SiO_2@NBD-CP@PEG, entry 5 in Table 1) and the dual fluorescent 2,4-D-MIP/CP particles without PEG brushes [briefly the ungrafted (dual fluorescent) 2,4-D-MIP/CP] (i.e., rQD-SiO_2@NBD-MIP/CP, entries 2 and 3 in Table 1) were also prepared similarly except for omitting 2,4-D and PEG-Br during the SI-ATRP processes, respectively. The resulting grafted and ungrafted dual fluorescent 2,4-D-MIPs/CPs showed certain weight increases compared with the starting rQD-SiO_2-Br (entries 1–5, Table 1), indicating the success of the above controlled surface imprinting processes via (one-pot) SI-ATRP. It is noteworthy here that some polymerization parameters

(including the ratio of 2,4-D to 4-VP, the amount of MA-Urea-NBD, and the amount of PEG-Br) were optimized to obtain the optimal imprinting effect, visual detection ability, and biological sample-compatibility for the grafted dual fluorescent 2,4-D-MIP, respectively.

AFM characterization results revealed that rQD-SiO_2-Br and the grafted and ungrafted 2,4-D-MIP/CP particles were uniform microspheres with number-average diameters ($D_{n,AFM}$) between 651 and 694 nm and size distribution indices (U) ≤ 1.012 (Fig. 2, Table 1). In addition, both the ungrafted and grafted 2,4-D-MIP/CP particles had larger diameters than rQD-SiO_2-Br particles (Table 1). DLS analyses also confirmed the same particle size trend for the above samples, although the particle diameters determined by DLS are somewhat larger than those determined by AFM (Table 1), just as reported previously [29]. These results, together with the presence of some new absorption bands [i.e., C = O stretching band around 1731 cm^{-1} from the incorporated poly(EGDMA) and C = N stretching band around 1598 cm^{-1} from the incorporated poly(4-VP)] in the FT-IR spectra of the ungrafted and grafted 2,4-D-MIPs/CPs in comparison with that of rQD-SiO_2-Br and the occurrence of the new CH_2 bending vibration band around 1450 cm^{-1} (from PEG) in the spectra of the grafted 2,4-D-MIP/CP compared with those of the ungrafted ones (Fig. 3), the presence of one fluorescence peak around 515 nm and another one around 710 nm in the fluorescent spectra of the ungrafted and grafted 2,4-D-MIPs/CPs (see the representative fluorescence spectrum of the grafted 2,4-D-MIP in Fig. 1(c)), the dramatically enhanced static water contact angles of the ungrafted 2,4-D-MIP/CP films in comparison with that of the rQD-SiO_2-Br film and largely reduced static water contact angles of the grafted 2,4-D-MIP/CP films compared with the ungrfated ones (Table 1), and the formation of hollow polymer particles by etching silica cores from the ungrafted and grafted 2,4-D-MIP/CP particles with

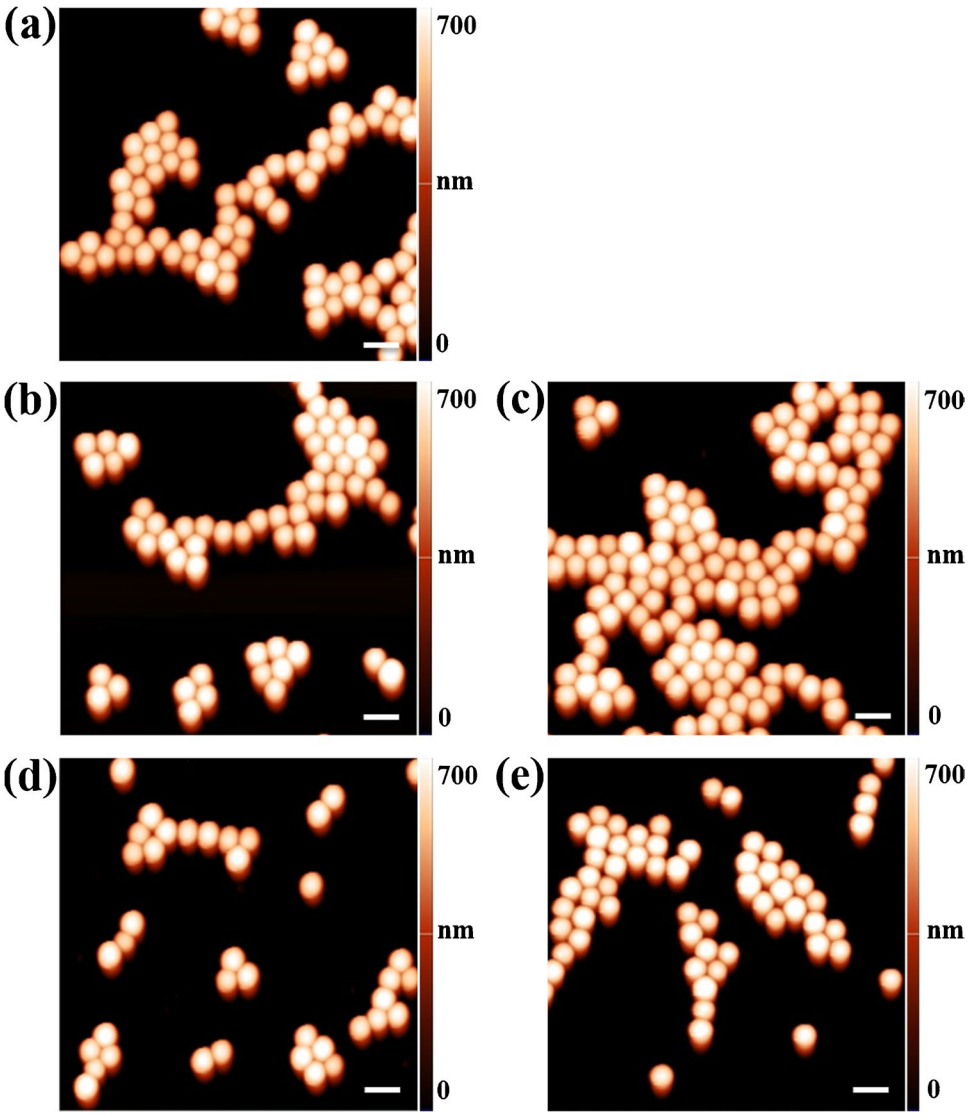

Fig. 2 AFM height images of rQD-SiO_2-Br (**a**), rQD-SiO_2@NBD-MIP (**b**), rQD-SiO_2@NBD-CP (**c**), rQD-SiO_2@NBD-MIP@PEG (**d**), and rQD-SiO_2@NBD-CP@PEG (**e**). The scale bar is 1 μm

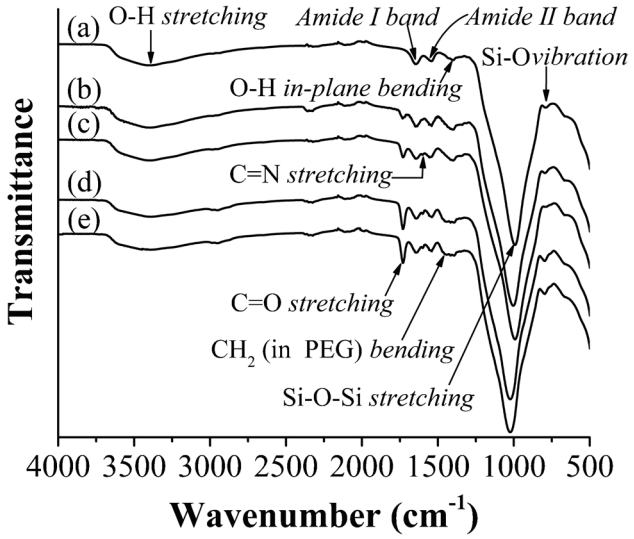

Fig. 3 FT-IR spectra of rQD-SiO_2-Br (**a**), rQD-SiO_2@NBD-MIP (**b**), rQD-SiO_2@NBD-CP (**c**), rQD-SiO_2@NBD-MIP@PEG (**d**), and rQD-SiO_2@NBD-CP@PEG (**e**)

a hydrogen fluoride (HF) solution in ethanol (Fig. S3), strongly verified the successful synthesis of our desired grafted and ungrafted dual fluorescent 2,4-D-MIPs/CPs.

Equilibrium/competitive binding properties of the ungrafted and grafted dual fluorescent 2,4-D-MIPs/CPs

The equilibrium template bindings of the ungrafted and grafted dual fluorescent 2,4-D-MIPs/CPs were first studied in both the organic solvent (acetonitrile) and the undiluted pure bovine milk. It can be seen from Fig. S4a that both the ungrafted and grafted 2,4-D-MIPs showed obvious specific template binding (i.e., the binding difference between the MIP and its CP [30]) in acetonitrile, revealing that the imprinted binding sites are present in these MIPs. On the other hand, negligible specific template binding was observed for the ungrafted 2,4-D-MIP in pure bovine milk, mainly because of its rather high surface hydrophobicity [31]. In sharp contrast, the grafted 2,4-D-MIP exhibited a specific binding in pure bovine milk almost the same as it showed in acetonitrile (Fig. S4a,b), mainly because of its largely improved surface hydrophilicity [31].

The binding selectivity of the ungrafted and grafted dual fluorescent 2,4-D-MIPs/CPs was then evaluated by measuring their competitive bindings toward 2,4-D and its structural analogues [POAc and CPOAc (Fig. 1(d))] in different media (Fig. S5). Although both the ungrafted and grafted 2,4-D-MIPs showed apparent 2,4-D selectivity in acetonitrile, only the grafted 2,4-D-MIP exhibited selective 2,4-D binding in pure bovine milk (Table S1). The above results strongly demonstrate that our one-pot SI-ATRP strategy is highly versatile for obtaining complex biological sample-compatible MIPs.

Direct and highly selective optosensing of 2,4-D in the undiluted pure bovine milk with the grafted dual fluorescent 2,4-D-MIP/CP

The photostability and reusability of the grafted dual fluorescent 2,4-D-MIP/CP were first evaluated because of their high importance for the practical uses of such optosensing materials. The fluorescence intensities of the aqueous dispersions of both the grafted dual fluorescent 2,4-D-MIP and 2,4-D-CP [including those of their incorporated red CdTe QDs (around 710 nm) and green NBD fluorophores (around 515 nm)] hardly changed after being put at room temperature under air atmosphere for 10 days (Fig. S6a,b), demonstrating their high photostability. Moreover, their excellent reusability was also confirmed by their nearly constant fluorescent intensities during 10 regeneration cycles (Fig. S7a,b).

The binding kinetics of the grafted dual fluorescent 2,4-D-MIP/CP were evaluated by studying the time-dependence of the fluorescence intensities of their mixtures with 2,4-D in the undiluted pure bovine milk. The grafted dual fluorescent 2,4-D-MIP/CP showed a continuous increase in the fluorescence intensities of NBD fluorophores around 515 nm but negligible change in the fluorescence intensities of CdTe QDs around 710 nm over time upon exposing to 2,4-D in pure bovine milk (Figs. 4(a) and S8), just as reported in our previous reports [21, 22]. The fluorescence intensities of NBD fluorophores embedded inside the grafted dual fluorescent 2,4-D-MIP/CP reached their maximum values around 30 min, revealing that they have fast binding kinetics. In particular, the grafted dual fluorescent 2,4-D-MIP showed much larger fluorescence enhancement effect than 2,4-D-CP, which again demonstrates the presence of imprinted binding sites inside the grafted dual fluorescent MIP (thus leading to its much stronger affinity toward 2,4-D than 2,4-D-CP).

Next, the spectrofluorimetric titration experiments of the grafted dual fluorescent 2,4-D-MIP/CP were carried out in the undiluted pure bovine milk to obtain the optosensing parameters including the linear detection range and limit of detection (LOD). While both the grafted dual fluorescent 2,4-D-MIP and its CP showed negligible change in the fluorescence intensities of CdTe QDs around 710 nm upon exposing to different concentrations of 2,4-D, they displayed continuous enhancement in the fluorescence intensities of NBD fluorophores around 515 nm with increasing the 2,4-D concentration (Fig. 5(a,b)). Much larger fluorescence enhancement effect (at 515 nm) was also observed for the studied 2,4-D-MIP than 2,4-D-CP. The grafted

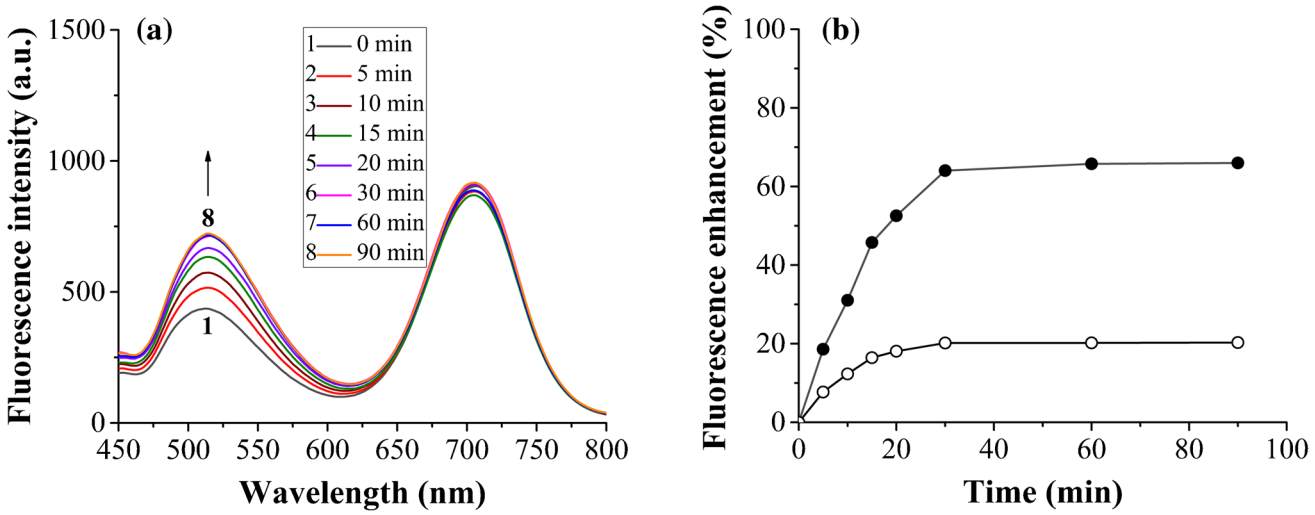

Fig. 4 (**a**) Fluorescence spectra of the grafted dual fluorescent 2,4-D-MIP (0.25 mg/mL) after its incubation with a 2,4-D solution (25 μM) in pure bovine milk at 25 °C for different times. (**b**) Binding kinetics of the grafted dual fluorescent 2,4-D-MIP (filled symbol)/CP (open symbol) (0.25 mg/mL) in a 2,4-D solution (25 μM) in pure milk at 25 °C (derived from Figs. 4(a) and S8; fluorescence enhancement (%) = $[(F_t - F_0)/F_0)] \times 100$, where F_t and F_0 are the fluorescence intensity of the green NBD unit (at 515 nm) at a time of t and 0, respectively)

dual fluorescent 2,4-D-MIP thus showed not only largely enhanced fluorescence intensity ratios of NBD fluorophores (at 515 nm) to CdTe QDs (at 710 nm) (i.e., F_{515}/F_{710}) but also an obvious fluorescence color change from red to blue-green (under 365 nm UV light irradiation) (the inset of Fig. 5(a)) with increasing the 2,4-D concentration from 0 to 100 μM.

In contrast, much smaller F_{515}/F_{710} enhancement and negligible fluorescence color change were found for the grafted dual fluorescent 2,4-D-CP under the same condition (the inset of Fig. 5(b)). By fitting the above spectrofluorimetric titration results with Stern–Volmer equation (or plotting $(F_{515}/F_{710})/(F_{515}/F_{710})_0$ versus 2,4-D concentration), we obtained a linear detection range from 0 to 25 μM [$y = 0.034x + 0.975$, where y refers to $(F_{515}/F_{710})/(F_{515}/F_{710})_0$ and x is the 2,4-D concentration; Fig. 5(c)] and a LOD of 0.12 μM [LOD = $3\delta/k_{MIP}$, where δ is the standard deviation of the blank measurements (for 20 times) and k_{MIP} is the slope of the linear calibration plot (i.e., 0.034) [32]] for the grafted dual fluorescent 2,4-D-MIP in pure milk. This LOD value is lower than the maximum contaminant level of 2,4-D in drinking water (i.e., 0.32 μM or 70 μg L^{-1}) set by the WHO and US EPA [33, 34]. Note that the LOD value (in pure milk) of our grafted dual fluorescent 2,4-D-MIP prepared via one-pot SI-ATRP is comparable with those (0.13 μM) of our previously reported grafted dual fluorescent 2,4-D-MIPs prepared via either two-step SI-ATRP [22] or the combined use of two-step SI-RAFT polymerization and coupling chemistry [21]. The imprinting factor of this grafted dual fluorescent 2,4-D-MIP was derived to be 3.8 in pure bovine milk through dividing the slope of the linear calibration plot for MIP (k_{MIP}) by that for CP (k_{CP}). The above results again confirmed the existence of imprinted binding sites in the grafted dual fluorescent 2,4-D-MIP and its high complex biological sample-compatibility.

In this context, it is also noteworthy that the ungrafted dual fluorescent 2,4-D-MIP showed negligible fluorescence enhancement at 515 nm upon its exposure to different concentrations of 2,4-D in pure bovine milk (Fig. S10a), although it showed dramatic fluorescence enhancement at 515 nm upon exposing to 2,4-D in the organic solvent (Fig. S9a). This phenomenon should stem from the rather high surface hydrophobicity of the ungrafted dual fluorescent 2,4-D-MIP (Table 1), which could lead to the significant adsorption of the proteins in pure bovine milk onto the ungrafted MIP surfaces, and thus the blockage of its imprinted sites. The above results further verify the high versatility of our one-pot SI-ATRP strategy for preparing MIP optosensors fully compatible with complex biological samples.

Finally, the fluorescence enhancement effects of the grafted dual fluorescent 2,4-D-MIP/CP upon their exposure to 2,4-D and its structurally related analogue POAc, CPOAc, or DCPAc (Fig. 1(d)) as well as some inorganic species such as $CaCl_2$, $ZnCl_2$, or NaCl and several other organic compounds such as glucose, vitamin C, lactose, or bovine serum albumin (BSA) in pure bovine milk were studied to evaluate their optosensing selectivity. It can be seen from Fig. 6(a,c) that the grafted dual fluorescent 2,4-D-MIP showed much larger fluorescence enhancement toward 2,4-D than its analogues and the above-mentioned inorganic species and other organic compounds. This,

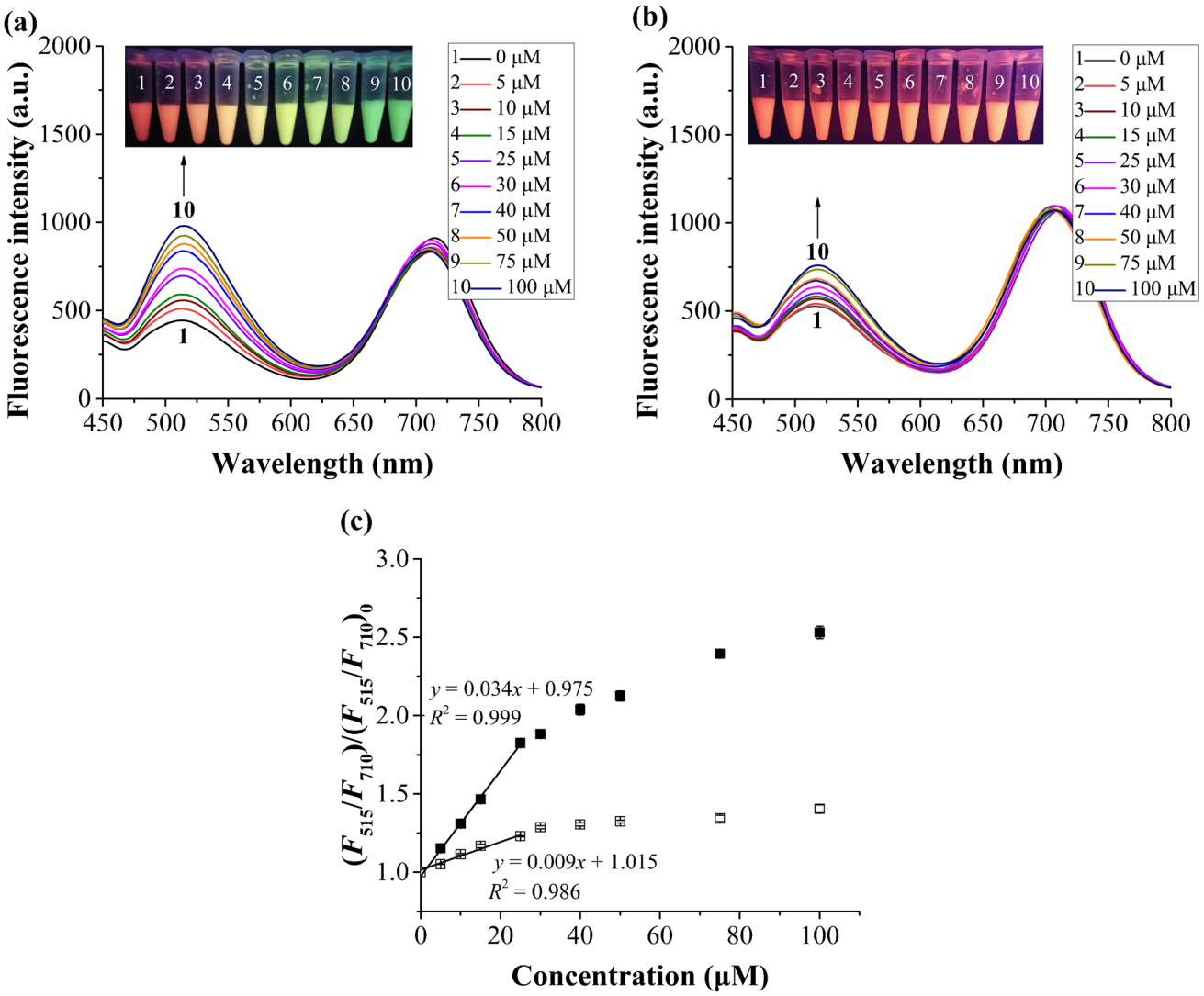

Fig. 5 (**a**, **b**) Fluorescence spectra of the grafted dual fluorescent 2,4-D-MIP (**a**) and 2,4-D-CP (**b**) (0.25 mg/mL) upon their exposure to different concentrations of 2,4-D in pure bovine milk at 25 °C for 2 h (inset: fluorescence color changes of the MIP/CP upon their exposure to different concentrations of 2,4-D). (**c**) Dependence of the fluorescence enhancement $[(F_{515}/F_{710})/(F_{515}/F_{710})_0$, where (F_{515}/F_{710}) and $(F_{515}/F_{710})_0$ are the fluorescence intensity ratio of NBD fluorophores to CdTe QDs in the presence and absence of 2,4-D, respectively] of the grafted dual fluorescent 2,4-D-MIP (filled symbol)/2,4-D-CP (open symbol) on the 2,4-D concentration (derived from Fig. 5(a,b))

together with the almost same and rather small fluorescence enhancement of the grafted dual fluorescent 2,4-D-MIP and 2,4-D-CP toward all the analogues of 2,4-D and the other inorganic and organic compounds, clearly demonstrates that the studied 2,4-D-MIP has high 2,4-D optosensing selectivity and its fluorescence enhancement toward the analogues of 2,4-D, and the other inorganic and organic compounds mainly stems from nonspecific bindings. In particular, the addition of the same amount of POAc, CPOAc, or DCPAc or two equivalent of $CaCl_2$, $ZnCl_2$, NaCl, glucose, vitamin C, lactose, or BSA into 2,4-D solutions hardly had any influence on the fluorescent responses of the grafted dual fluorescent 2,4-D-MIP toward 2,4-D (Fig. 6(b,d)), further confirming the excellent optosensing selectivity of this 2,4-D-MIP in the complex biological milieu.

Direct, selective, and accurate quantification of 2,4-D in the undiluted pure goat milk with the grafted dual fluorescent 2,4-D-MIP

The grafted dual fluorescent 2,4-D-MIP was also applied to detect 2,4-D in the undiluted pure goat milk to demonstrate its general applicability for direct and highly selective optosensing of 2,4-D in complex biological samples. The commercially available goat milk was first spiked with different amounts of 2,4-D and then used for

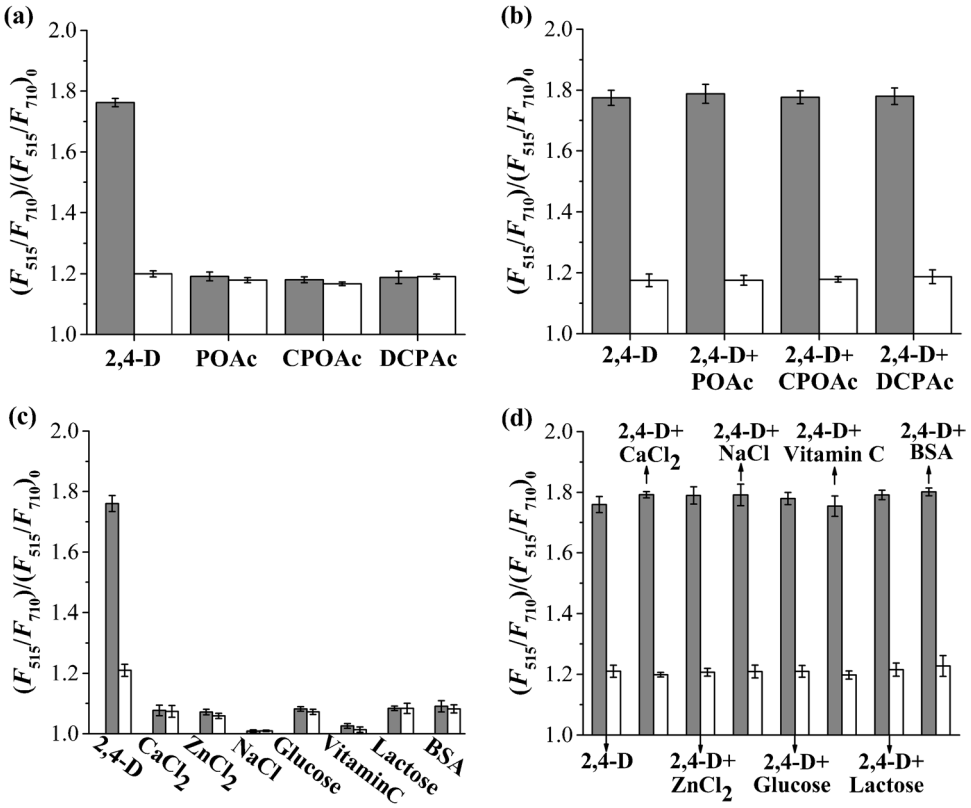

Fig. 6 Fluorescence enhancement of the grafted dual fluorescent 2,4-D-MIP (filled column)/2,4-D-CP (open column) (0.25 mg/mL) upon exposing to a 2,4-D, POAc, CPOAc, or DCPAc solution ($C_{2,4\text{-D, POAc, CPOAc, or DCPAc}}$ = 25 μM) (**a**), or to a 2,4-D solution (25 μM) in the presence of the same concentration of POAc, CPOAc, or DCPAc (**b**), or to a $CaCl_2$, $ZnCl_2$, NaCl, glucose, vitamin C, lactose, or BSA solution (C_{CaCl2}, $ZnCl_2$, NaCl, glucose, Vitamin C, lactose, or BSA = 25 μM) (**c**), or to a 2,4-D solution (25 μM) in the presence of 50 μM of $CaCl_2$, $ZnCl_2$, NaCl, glucose, vitamin C, lactose, or BSA (**d**) in pure bovine milk at 25 °C for 2 h

the recovery tests. Good recoveries (96.0–102.0%) and low relative standard deviations (RSDs) (0.7–4.0%) were achieved for 2,4-D optosensing (entries 1–3, Table 2). In addition, the use of the grafted dual fluorescent 2,4-D-MIP for optosensing 2,4-D in pure goat milk samples spiked with mixtures of 2,4-D and some interfering substances (including POAc, CPOAc, and DCPAc) also led to satisfactory recoveries (98.2–104.0%) and high detection accuracy (RSD = 1.3–3.4%) (entries 4–6, Table 2). In particular, these 2,4-D optosensing results were found to be in good agreement with the HPLC measurement results (Table 2) [a sample pretreatment

Table 2 Direct quantification of 2,4-D in the undiluted pure goat milk at three spiking levels of both 2,4-D and its mixtures with several analogues with the grafted dual fluorescent 2,4-D-MIP

Entry	Analyte(s)	Concentrations of analyte(s) (μM)		Optosensing recovery ± RSD (%) (n = 3)	HPLC recovery ± RSD (%) (n = 3)
		Spiked	Found (2,4-D) (optosensing)		
1	2,4-D	0.5	0.48 ± 0.02	96.0 ± 4.0	103.6 ± 2.6
2	2,4-D	5	5.10 ± 0.13	102.0 ± 2.6	98.7 ± 3.9
3	2,4-D	10	10.10 ± 0.07	101.0 ± 0.7	102.5 ± 2.1
4	2,4-D + POAc + CPOAc + DCPAc	0.5(2,4-D) + 0.5POAc + 0.5CPOAc + 0.5DCPAc	0.51 ± 0.01	102.0 ± 2.0	98.0 ± 2.8
5	2,4-D + POAc + CPOAc + DCPAc	5(2,4-D) + 5POAc + 5CPOAc + 5DCPAc	4.91 ± 0.17	98.2 ± 3.4	102.4 ± 2.2
6	2,4-D + POAc + CPOAc + DCPAc	10(2,4-D) + 10POAc + 10CPOAc + 10DCPAc	10.4 ± 0.13	104.0 ± 1.3	96.0 ± 1.3

procedure (i.e., removing proteins by adding acetonitrile into milk samples following our previously reported method [29]) was carried out prior to HPLC (with a UV–Vis detector) analyses]. The above results definitely demonstrate that the hydrophilic "turn-on"-type ratiometric fluorescent MIP prepared via our one-pot SI-ATRP can be used for direct, selective, and accurate 2,4-D optosensing in complex biological samples without requiring any sample pretreatment and expensive instrument.

It is worth mentioning here that our presently developed grafted dual fluorescent 2,4-D-MIP optosensor exhibits obvious advantages over the previously reported MIP-based (Table S2) or other nanomaterial-based 2,4-D-detecting systems (Table S3) because it does not need any complicated and time-consuming sample pretreatment or high dilution procedure for the analyses of complex biological samples. This, together with its high enough analytical sensitivity (its LOD value is lower than the maximum contaminant level of 2,4-D in drinking water regulated by the WHO and US EPA [33, 34]) as well as excellent selectivity and detection accuracy, makes it highly promising in the real-world bioanalyses and diagnostics.

Conclusions

A highly efficient new strategy has been successfully developed for preparing "turn-on"-type ratiometric fluorescent MIP microspheres capable of directly and selectively optosensing 2,4-D in the undiluted pure milks, which involves the controlled grafting of a green NBD-labeled 2,4-D-MIP layer with hydrophilic polymer brushes onto the preformed "living" red CdTe QD-labeled silica particles via one-pot SI-ATRP in the presence of a PEG macro-ATRP initiator. The combined advantages of MIPs and "turn-on"-type ratiometric fluorescent analyses endowed these dual fluorescent 2,4-D-MIP particles with high optosensing selectivity and sensitivity as well as direct visual detection ability in the undiluted pure milks. They also showed outstanding photostability/reusability and excellent applicability for the direct and highly selective herbicide detection in the undiluted pure goat milk. The high controllability of the one-pot SI-ATRP, together with the easy one-pot synthesis of uniform "living" CdTe QD-labeled silica particles (or other monodisperse "living" polymer particles via atom transfer radical precipitation polymerization [23]), makes this new strategy highly efficient for preparing various complex biological sample-compatible MIP optosensors that are of great potential in a wide range of real-world bioanalytical and diagnostic applications. Our recent experimental results have demonstrated that this new strategy can also be applied for preparing complex biological sample-compatible ratiometric MIPs for other organic acid templates. Further investigation is ongoing to introduce more efficient ATRP techniques [e.g., activators regenerated by electron transfer for atom transfer radical polymerization (ARGET-ATRP) [35]] for this strategy to improve its versatility.

Supplementary Information The online version contains supplementary material available at https://doi.org/10.1007/s00604-022-05551-8.

Funding This work was financially supported by the National Natural Science Foundation of China (21574070 and 22071121) and the Project supported by the NCC Fund (NCC2020PY12).

Declarations

Conflict of interest The authors declare no competing interests.

References

1. Zhang H, Ye L, Mosbach K (2006) Non-covalent molecular imprinting with emphasis on its application in separation and drug development. J Mol Recognit 19:248–259
2. Hoshino Y, Shea KJ (2011) The evolution of plastic antibodies. J Mater Chem 21:3517–3521
3. Takeuchi T, Sunayama H (2018) Beyond natural antibodies-a new generation of synthetic antibodies created by post-imprinting modification of molecularly imprinted polymers. Chem Commun 54:6243–6251
4. Zhang H (2020) Molecularly imprinted nanoparticles for biomedical applications. Adv Mater 32:1806328
5. Xu S, Wang L, Liu Z (2020) Molecularly imprinted polymer nanoparticles: an emerging versatile platform for cancer therapy. Angew Chem Int Ed 60:3858–3869
6. Tse Sum Bui B, Auroy T, Haupt K (2022) Fighting antibiotic-resistant bacteria: promising strategies orchestrated by molecularly imprinted polymers. Angew Chem Int Ed 61:e202106493
7. Basabe-Desmonts L, Reinhoudt DN, Crego-Calama M (2007) Design of fluorescent materials for chemical sensing. Chem Soc Rev 36:993–1017
8. Haupt K, Mosbach K (2000) Molecularly imprinted polymers and their use in biomimetic sensors. Chem Rev 100:2495–2504
9. Canfarotta F, Whitcombe MJ, Piletsky SA (2013) Polymeric nanoparticles for optical sensing. Biotechnol Adv 31:1585–1599
10. Wackerlig J, Lieberzeit PA (2015) Molecularly imprinted polymer nanoparticles in chemical sensing-synthesis, characterisation and application. Sensor Actuat B-Chem 207:144–157
11. Wan W, Wagner S, Rurack K (2016) Fluorescent monomers: "bricks" that make a molecularly imprinted polymer "bright." Anal Bioanal Chem 408:1753–1771
12. Yang Q, Li J, Wang X, Peng H, Xiong H, Chen L (2018) Strategies of molecular imprinting-based fluorescence sensors for chemical and biological analysis. Biosens Bioelectron 112:54–71
13. Zhang H (2021) Water-compatible fluorescent molecularly imprinted polymers. In: Martín-Esteban A (ed) Methods in molecular biology 2359: Molecularly Imprinted Polymers-Methods and Protocols. Humana Press (Springer Nature), New York, pp 97–108
14. Wang X, Yu J, Wu X, Fu J, Kang Q, Shen D, Li J, Chen L (2016) A molecular imprinting-based turn-on ratiometric fluorescence sensor for highly selective and sensitive detection of 2,4-dichlorophenoxyacetic acid (2,4-D). Biosens Bioelectron 81:438–444

15. Lu H, Xu S (2017) Visualizing BPA by molecularly imprinted ratiometric fluorescence sensor based on dual emission nanoparticles. Biosens Bioelectron 92:147–153
16. Lian Z, Zhao M, Wang J, Yu RC (2021) Dual-emission ratiometric sensor based molecularly imprinted nanoparticles for visual detection of okadaic acid in seawater and sediment. Sensor Actuat B-Chem 346:130465
17. Sun X, Jiang M, Chen L, Niu N (2021) Construction of ratiometric fluorescence MIPs probe for selective detection of tetracycline based on passion fruit peel-carbon dots and europium. Microchim Acta 188:297
18. Hu X, Guo Y, Zhang J, Wang X, Fang G, Wang S (2022) A signal-amplified ratiometric fluorescence biomimetic sensor based on the synergistic effect of IFE and AE for the visual smart monitoring of oxytetracycline. Chem Eng J 433:134499
19. Li W, Zhang H, Chen S, Liu Y, Zhuang J, Lei B (2016) Synthesis of molecularly imprinted carbon dot grafted YVO_4:Eu^{3+} for the ratiometric fluorescent determination of paranitrophenol. Biosens Bioelectron 86:706–713
20. Yang Q, Li C, Li J, Wang X, Arabi M, Peng H, Xiong H, Chen L (2020) Rational construction of a triple emission molecular imprinting sensor for accurate naked-eye detection of folic acid. Nanoscale 12:6529–6536
21. Hou Y, Zou Y, Zhou Y, Zhang H (2020) Biological sample-compatible ratiometric fluorescent molecularly imprinted polymer microspheres by RAFT coupling chemistry. Langmuir 36:12403–12413
22. Xu S, Zou Y, Zhang H (2020) Well-defined hydrophilic "turn-on"-type ratiometric fluorescent molecularly imprinted polymer microspheres for direct and highly selective herbicide optosensing in the undiluted pure milks. Talanta 211:120711
23. Zhang H (2013) Controlled/"living" radical precipitation polymerization: a versatile polymerization technique for advanced functional polymers. Eur Polym J 49:579–600
24. Zhao M, Chen X, Zhang HT, Yan H, Zhang H (2014) Well-defined hydrophilic molecularly imprinted polymer microspheres for efficient molecular recognition in real biological samples by facile RAFT coupling chemistry. Biomacromolecules 15:1663–1675
25. Ton XA, Tse Sum Bui B, Resmini M, Bonomi P, Dika I, Soppera O, Haupt K (2013) Versatile fiber-optic fluorescence sensor based on molecularly imprinted microstructures polymerized in situ. Angew Chem Int Ed 52:8317–8321
26. Yang Y, Niu H, Zhang H (2016) Direct and highly selective drug optosensing in real, undiluted biological samples with quantum-dot-labeled hydrophilic molecularly imprinted polymer microparticles. ACS Appl Mater Interfaces 8:15741–15749
27. Fischer H (1997) The persistent radical effect in "living" radical polymerization. Macromolecules 30:5666–5672
28. Zhang H, Klumperman B, Ming W, Fischer H, van der Linde R (2001) Effect of Cu(II) on the kinetics of the homogeneous atom transfer radical polymerization of methyl methacrylate. Macromolecules 34:6169–6173
29. Ma Y, Pan G, Zhang Y, Guo X, Zhang H (2013) Narrowly dispersed hydrophilic molecularly imprinted polymer nanoparticles for efficient molecular recognition in real aqueous samples including river water, milk, and bovine serum. Angew Chem Int Ed 52:1511–1514
30. Boonpangrak S, Whitcombe MJ, Prachayasittikul V, Mosbach K, Ye L (2006) Preparation of molecularly imprinted polymers using nitroxide-mediated living radical polymerization. Biosens Bioelectron 22:349–354
31. Zhang H (2014) Water-compatible molecularly imprinted polymers: promising synthetic substitutes for biological receptors. Polymer 55:699–714
32. Apodaca DC, Pernites RB, Ponnapati RR, Del Mundo FR, Advincula RC (2011) Electro polymerized molecularly imprinted polymer films of a bis-terthiophene dendron: folic acid quartz crystal microbalance sensing. ACS Appl Mater Interfaces 3:191–203
33. Hamilton D, Ambrus A, Dieterle R, Felsot A, Harris C, Holland P, Katayama A, Kurihara N, Linders J, Unsworth J, Wong S (2003) Regulatory limits for pesticide residues in water (IUPAC technical report). Pure Appl Chem 75:1123–1155
34. Han DM, Jia WP, Liang HD (2010) Selective removal of 2,4-dichlorophenoxyacetic acid from water by molecularly-imprinted amino-functionalized silica gel sorbent. J Environ Sci 22:237–241
35. Jakubowski W, Min K, Matyjaszewski K (2006) Activators regenerated by electron transfer for atom transfer radical polymerization of styrene. Macromolecules 39:39–45